Understanding Aluminum Location and Non-framework Ions Effects on Alkane Adsorption in Aluminosilicates: A Molecular Simulation Study

Bei Liu,[†] Elena García-Pérez,[‡] David Dubbeldam,[§] Berend Smit,[†,||] and Sofía Calero*[,‡]

Van't Hoff Institute for Molecular Sciences, University of Amsterdam, Nieuwe Achtergracht 166, 1018 WV Amsterdam, The Netherlands, Department of Physical, Chemical, and Natural Systems, University Pablo de Olavide, Ctra. Utrera km. 1. 41013, Seville, Spain, Chemical and Biological Engineering Department, Northwestern University, Evanston, Illinois 60208, and Centre Européen de Calcul Atomique et Moléculaire (CECAM), Ecole Normale Supérieure, 46 allée d'Italie, 69007 Lyon, France

Received: December 5, 2006; In Final Form: May 16, 2007

In our previous work, a computational method to characterize framework aluminum in aluminosilicates was proposed (García-Pérez, E., et al. *Angew. Chem., Int. Ed.* **2007**, *46*, 276). In this work, the method was adopted to identify the most likely positions of aluminum in TON, FER, and MOR zeolites and to understand their different adsorption behaviors in detail. The simulations show that the location of aluminum affects the positions of the ions, and thus influences the adsorption. With the determined structures, the effects of non-framework ions on the adsorption behaviors of alkanes in these zeolites were studied systematically and the relations of the macroscopic adsorption behaviors of alkanes to their microscopic structures were elucidated. The results provided a better understanding of the influences of the position and density of aluminum on adsorption in zeolites from a microscopic level that may guide the future rational synthesis of new structures.

1. Introduction

Zeolites are microporous materials that have found wide applications as efficient heterogeneous catalysts and adsorbents in the petrochemical industry. In these materials the adsorption and diffusion of hydrocarbons in the zeolite pores play an important role.[1,2] The structure of zeolites is composed of silicon and aluminum oxide tetrahedra and charge-balancing ions. The presence of ions influences the adsorption properties of the zeolites. As the positions and stability of ions in the zeolites are strongly related to their Al distributions,[3] it is therefore important to identify the aluminum site locations. Whereas it is relatively easy to determine the Si/Al ratio of the material, it is much more difficult to locate the exact positions of the aluminum atoms in the framework experimentally.[4−9] These difficulties motivate us to complement the experimental efforts with modeling and simulations.

H-TON, H-FER, and Na-MOR are structures used for industrial applications and many experimental investigations have been performed on the adsorption properties of these zeolites.[10−30] In these studies the positions of the aluminum atoms in these materials are not very clear, and the understanding of the effects of non-framework ions on the adsorption properties at the molecular level is yet incomplete. To date, all the simulations[31−39] about the adsorption properties of alkanes have been performed on the pure silica representation of TON and FER zeolites and only a limited simulations[26,40−42] on Na-MOR zeolites. In this work we perform a systematic study on these materials by molecular simulations to reveal the underlying mechanisms at a microscopic level.

* Corresponding author. E-mail: scaldia@upo.es.
[†] University of Amsterdam.
[‡] University Pablo de Olavide.
[§] Northwestern University.
[||] Ecole Normale Supérieure.

The aluminum distribution on the crystal level, as well as the distribution on the level of a single unit cell, remains a subject of much debate and continued research efforts.[43−49] Macroscopically, the amount of aluminum might vary from the center of the crystal to the outer edges, while microscopically the Löwenstein rule, that is, two negatively charged Al atoms can never bond the same O atom, is well established. Our approach implicitly assumes a homogeneous aluminum distribution for the entire zeolite. To obtain some insights in the effect of variations of the amount of aluminum around an average value, we estimated the Henry coefficients of model materials in which some unit cells contain slightly less and others slightly more aluminum concentrations. These calculations agreed very well with those for a uniform aluminum distribution, giving us some confidence that we can compare our results with experimental samples.

The remainder of the paper is organized as follows. In section 2, we present the details of our simulation methodology, including descriptions of the zeolite models, the force fields, and the simulation technique used. In section 3, computed Henry coefficients, adsorption isotherms, and heats of adsorption for linear alkanes in several zeolite structures are given, and those in H-TON, H-FER, and Na-MOR zeolites are analyzed and discussed in detail. Finally, some concluding remarks are given in section 4.

2. Simulation Models and Methods

2.1. Zeolite Models. The structures of zeolites considered in this work are well-known and have been used in many previous simulation studies. The pure silica structures were constructed by using the crystallographic coordinates reported[50] and the structures with aluminum were obtained by randomly replacing silicon by aluminum atoms, satisfying the Löwenstein rule.

10.1021/jp0683521 CCC: $37.00
Published on Web 06/21/2007

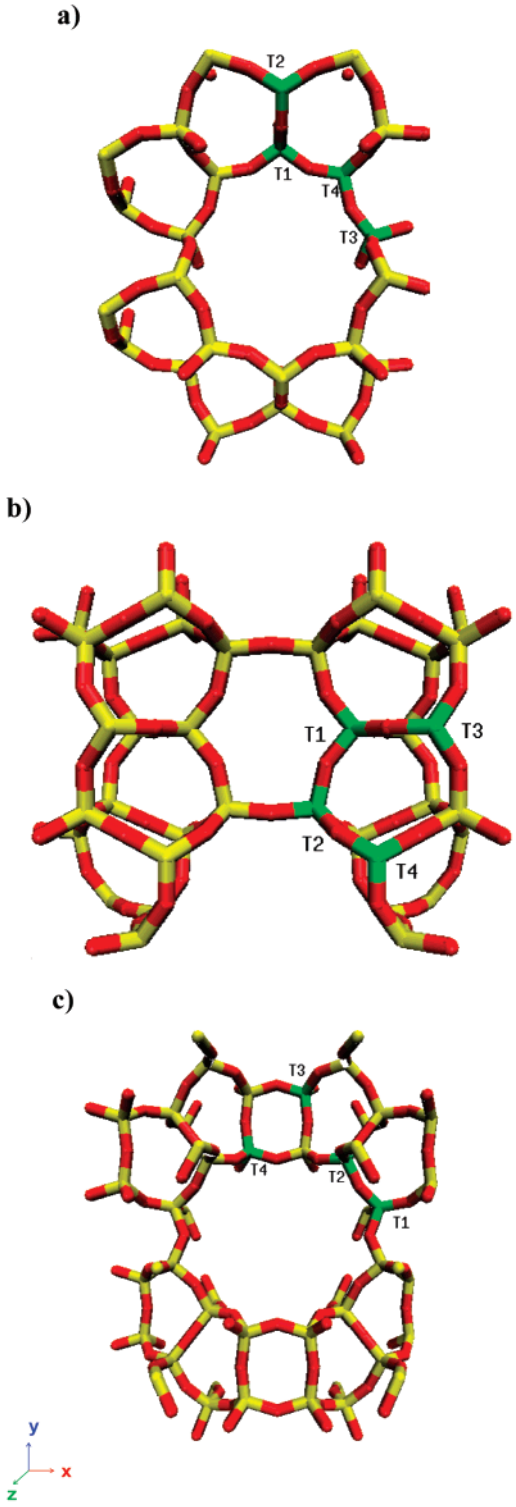

Figure 1. Representation of the model unit cell of (a) TON, (b) FER, and (c) MOR with distinct T-sites where Al atoms can be located.

Since TON, FER, and MOR zeolites were studied in detail in this work, their structures are shown in Figure 1, while the structures for the other zeolites considered can be found easily in the literature.[41,51−53] The TON-type zeolite exhibits a unidirectional 10-ring pore system along the *z*-axis, with a pore aperture of 5 Å. The FER-type zeolite consists of straight 10-ring channels (5.4 × 4.2 Å) parallel to the *z*-axis which are interconnected by cages with 8-ring windows (4.8 × 3.5 Å) in the *y*-direction. The MOR-type zeolite has main channels parallel to [001], having a slightly elliptical cross section with 12 TO_4 tetrahedron units (T = Si, Al), which are connected with small side channels parallel to [010], with 8 TO_4 cross sections called side pockets. Four distinct T-sites aluminum can be located in them, shown in Figure 1 as T1, T2, T3, and T4. The zeolite lattices were assumed to be rigid in the simulations, because the flexibility of the framework has a negligible influence on the adsorption of alkanes.[54]

2.2. Force Fields. Our simulations have been performed using a unique set of parameters defined by Dubbeldam et al. that accurately reproduce alkane−alkane and alkane-zeolite interactions in all silica structures.[55,56] Simulations in zeolites with aluminum in the framework require additional parameters for all interactions involving non-framework ions. Consequently the force fields recently proposed by Calero et al.[51,57] are used in this work for sodium cations and protons, both are the extended version of the force field of Dubbeldam et al. [55, 56] to include the effects of sodium cations and protons. In these force fields the nature, density, and mobility of the non-framework ions, the density of the framework aluminum, and all host−guest interactions are carefully taken into account. The alkanes are described with a united atom model, in which CH_4, CH_3, and CH_2 groups are considered as single, charge-less interaction centers.[58] The beads in the chain are connected by harmonic bonding potentials. A harmonic cosine bending potential models the bond bending between three neighboring beads, and a Ryckaert−Bellemans potential controls the torsional angle. The interactions between the adsorbates as well as the adsorbates and the zeolite are described by Lennard−Jones potentials and the interactions between the non-framework ions and the zeolite are modeled by Coulombic potentials. For a detailed description of the force fields, the reader is referred to refs 51, 55−57.

2.3. Simulation Technique. For the calculation of the Henry coefficients and the isosteric heats of adsorption at infinite dilution Q_{st}^0, we performed configurational-bias Monte Carlo (CBMC) simulations in the *NVT* ensemble. Each simulation consists of at least 4×10^7 steps, and in each cycle one move is chosen at random with a fixed probability 0.1 for a molecule translation, 0.1 for rotation around the center of mass, and 0.8 for regrowth of the entire molecule. During the simulation we compute the Rosenbluth factor and the internal energy ΔU, which are directly related to the Henry coefficients and the Q_{st}^0.[56,59]

Adsorption isotherms were calculated in the grand-canonical ensemble using the CBMC method. The CB-GCMC method simulates an open system specified by fixed temperature T, volume V, and fugacity f. We converted the imposed fugacity to the corresponding pressure using the Peng−Robinson equation of state. Four types of moves were carried out: translation, rotation, exchange of molecules between the zeolite and a molecule reservoir, and partial regrowth. All simulations included at least 2×10^7 steps. As the total number of ions is constant during simulations, only translation movements and regrowth at a random position in the zeolite are considered for these particles.

The statistical uncertainty was estimated by dividing each run into five blocks and calculating the standard deviation from the block averages. The standard deviation was within ±10% for every simulation. A detailed description of the simulation methods can be found in our previous work. [51]

3. Results and Discussion

3.1. Categorizing Zeolites according to the Sensitivity of Adsorption Properties to the Aluminum Distributions. In this work, we first categorized the commonly used zeolites (FAU,

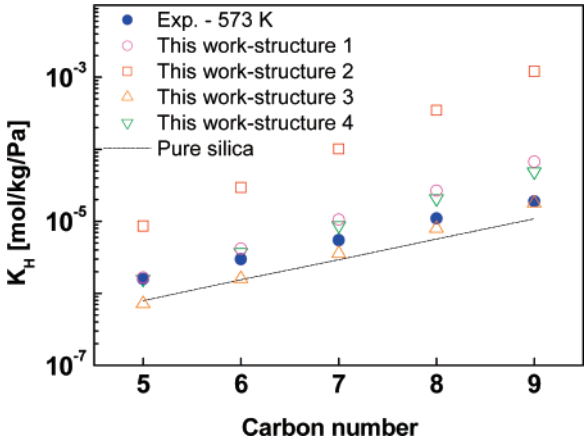

Figure 2. Comparison of the experimental[16] and simulated Henry coefficients of linear alkanes in H−TON zeolite at 573 K. Structures 1, 2, 3, and 4 indicate that the Al atom is located in T-site 1, 2, 3, and 4, respectively.

LTA, MEL, MFI, LTL, FER, MOR, and TON) into two groups according to the sensitivity of their adsorption properties to the aluminum distributions by computing the Henry coefficients of linear alkanes in them. In the simulations the Si/Al ratio is kept fixed by varying the aluminum distribution and using Na^+ and H^+ as non-framework ions. The results (see Supporting Information Figure 1) show that the adsorption properties of FAU, LTA, MEL, and MFI are insensitive to aluminum distribution and they can be included in the insensitive group, while LTL, FER, TON, and MOR belong to the sensitive class. Therefore, the first group of zeolites can be used to accurately parameterize our simulation method,[51,57] and for the second group of zeolites, their average aluminum distributions can be identified by matching the simulations with experiments using the parametrized simulation method.[60]

3.2. Aluminum Positions and Alkane Adsorptions in TON, FER, and MOR Zeolites. We have performed molecular simulations to identify the aluminum positions in TON, FER, and MOR zeolites, as well as to provide a better molecular understanding of the alkane adsorption in them. For these zeolites, experimental adsorption data are available, and it is feasible to consider all possible aluminum distributions per unit cell: $H_1^+[Al_1Si_{23}O_{48}]$-TON, $H_1^+[Al_1Si_{35}O_{72}]$-FER (both with 4 possible aluminum distributions per unit cell), and $Na_8^+[Al_8Si_{40}O_{96}]$-MOR (with 16 possible aluminum distributions per unit cell).

H-TON Zeolite. Figure 2 shows the calculated Henry coefficients of linear alkanes in H-TON zeolite at 573 K. The number of protons is kept one per unit cell to allow a direct comparison with experimental data. Since there are four distinct T-sites where aluminum can be located and as the positions and stability of protons in the zeolite are strongly related to its Al distribution,[3] four different structures were considered in this work, which correspond to the four T-sites. A comparison with the experimental values[16] indicates that most of the aluminum atoms on the zeolite sample are a combination of T3 and T4 substitutions for H-TON structures. Simulations at 473, 498, 523, and 548 K were also performed showing similar behavior (see ref 60 and Figure 2 in Supporting Information).

In order to clarify the differences among the structures, we examined the snapshots of these zeolites with adsorbed alkanes and those for hexane are shown in Figure 3. To illustrate the influences of protons on the adsorption, the results on pure silica structure are also shown for comparison. For pure silica structure, the hexane molecules adsorb homogeneously throughout the channels. In structures 1 and 4, protons were found located in the 10-ring channels partly. Protons take up adsorption volume in the channels where they are located but create additional preferred adsorption sites in the neighboring channels, which results in an increase of the adsorption comparing with the pure silica structure. As discussed in ref 57, the proton model necessarily assumes that there some traces of water in contact with the proton providing an effective adsorption volume that is significantly larger than one would expect from a single proton. We found that protons were all excluded from the 10-ring channels for structure 2, and they do increase the amount of adsorption in all 10-ring channels, leading to the highest adsorption capacity. The preferential location for proton in structure 3 is the 10-ring channels and the snapshot shows that protons occupy much volume in the channels, giving the lowest adsorption amount.

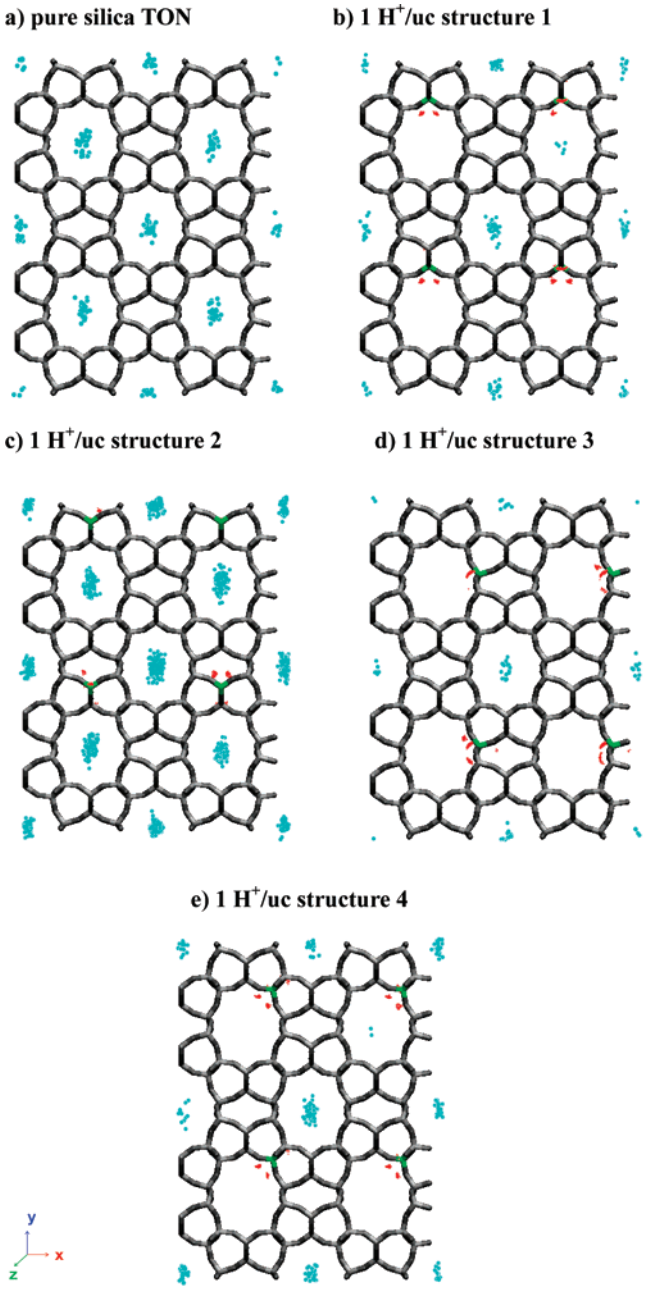

Figure 3. Distributions of hexane and the non-framework protons in TON zeolites at 5 kPa and 548 K. The centers of mass of the hexane molecules are represented by blue dots and the non-framework proton positions by red dots. The aluminum positions are indicated in green color.

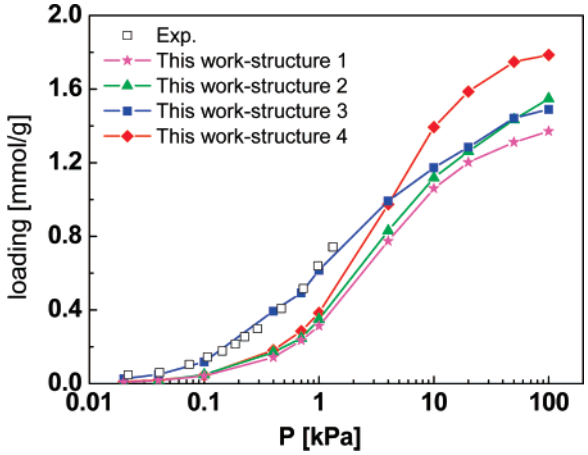

Figure 4. Comparison of the experimental[13] and simulated adsorption isotherms of propane in H-FER zeolite at 333 K. Structures 1, 2, 3, and 4 indicate that the Al atom is located in T-site 1, 2, 3, and 4, respectively.

TABLE 1: Comparison of the Experimental and Simulated Heats of Adsorption Q_{st}^0 [kJ/ mol] of C_3-C_6 in H-FER Zeolites

	propane	*n*-butane	*n*-pentane	*n*-hexane
experimental data[13]	49	59	69	79
this work	48.43	57.14	67.72	81.90

H-FER Zeolite. The adsorption behaviors of alkanes in H-FER zeolite were further investigated systematically. Figure 4 shows the calculated adsorption isotherms of propane at 333 K. Again the number of protons is kept one per unit cell and four different structures were considered corresponding to the four T-sites. Figure 4 shows that the calculated isotherms based on structure 3, that is, Al located on T3, agree very well with the experimental data. The adsorption isotherms of butane, pentane, and hexane show similar behavior (see ref 60 and Figure 3 in Supporting Information), illustrating that T3 structure is most likely the structure of the H-FER experimental sample. Heats of adsorption were also computed for this structure and comparison with experimental data[13] is provided in Table 1.

The snapshots of the different structures with adsorbed alkanes were examined and those for butane are given, as an example, in Figure 5. The snapshots show that butane molecules are distributed over the channels and the cages for all structures considered. For pure silica structure, butane molecules are located almost homogeneously between the channels and the cages. For structure 1, proton was found located in the 8-ring cages and butane molecules adsorbed preferentially in the 10-ring channels. Protons take up adsorption volume in the 8-ring cages but create additional preferred adsorption sites in the 10-ring channels, resulting in an increase of the adsorption. For structure 2, we found that the probability for protons located in the 8-ring cages and the 10-ring channels is almost the same, and from the snapshot, we can see that protons affect adsorption in a similar way as in structure 1, that is, decreasing the adsorption in the 8-ring cages but increasing it in the 10-ring channels. The preferential locations of protons in structure 3 are the 10-ring channels, which agrees well with the experimental analysis about the sample used in their work.[13] The protons occupy some volume in the 10-ring channels but the influence is not as big as in 8-ring cages. At low and intermediate loadings, they increase the amount of adsorption in both the 10-ring channels and the 8-ring cages, leading to the highest adsorption capacity. In structure 4, the preferential location for protons is the region across the 8-ring cages and the 10-ring channels, giving the lowest adsorption capacity. It seems that protons block the passageway to the 8-ring cages and the 10-ring channels.

The fractions of the adsorbed alkane molecules located in the FER 8-ring cages in structure 3 were calculated and the results are given in Figure 6 as a function of the loading. The ones on pure silica structure are also shown for comparison. Experimentally,[17,18] it is found that propane adsorbs preferentially in the 8-ring cage. The adsorption of pentane initially takes place only in the 10-ring channel and adsorption into the 8-ring cage occurs only at higher loadings. Hexane adsorbs only in the 10-ring channels and is excluded from the 8-ring cage. Our simulation results are consistent with the experimental observations. For butane, no preference is found by NMR measurements and our simulations predict that butane adsorption is preferred in the 10-ring channels for pure silica structure and in the 8-ring cage for H-FER structure. This can be explained by examining the snapshots of butane adsorption at low pressures. Figure 7 shows the sitting of butane in FER zeolites at 333 K and 0.05 kPa. For pure silica structure butane preferentially adsorbs in the 10-ring channels. Once we put any small amount inside the channels, they will start to repel *n*-alkanes attributed to the fact that the channel of FER-type zeolites is the smallest channel not to repel *n*-alkanes comparing with other zeolites.[61] When *n*-alkanes cannot reside in the 10-ring channel they will head for the 8-ring cage.

Na-MOR Zeolite. Another important zeolite considered in this work is Na-MOR zeolite. The adsorption isotherms and the Henry coefficients of methane in sixteen different structures were calculated and compared with available experimental data.[26,30] Our results show that the agreement with experimental values is remarkable for the structure where Al atoms replace Si 4, 18, 31, 42, 80, 93, 105, and 115.[60] In this structure the eight Al atoms are located in the 4-rings, in complete conformity with the suggested preferential sitting of aluminum provided by previous crystallographic, experimental, and theoretical work.[43,44,62−65] To study the effects of the cations on the adsorption behavior, we checked the snapshot of this structure with adsorbed methane at 323 K and 1 kPa, and compared with the adsorption in pure silica structure. The results are shown in Figure 8. For pure silica structure, the methane molecules are located almost homogeneously between the main channels and the side pockets. However, for the structure with cations, methane molecules were found adsorbed preferentially in the side pockets. Nearly half of the sodium cations were found to reside in the center of the 8-membered oxygen rings outside the main channels.[66,67] This agrees with the available experimental data.[68] Furthermore, the fraction of the adsorbed methane molecules located in the MOR main channels in the sodium and the pure silica structures was also calculated and the results are given in Figure 9 as a function of the loading. For pure silica structure, it is found that the side pockets are favored but not very strongly because the side pocket adsorption sites have a lower energy[26,69] and the percentage is almost constant with the increasing of the loading. For Na-MOR structure, side pocket adsorption becomes more favorable because the Na cations residing at the opening of the side pockets make these sites more attractive.[26] These results are in complete conformity with the snapshots shown in Figure 8 and with all previous results,[26,69] but those obtained by Smit and den Ouden.[40] Smit and den Ouden predicted exclusion of methane from the side pockets in Na-MOR structure considering that the side pockets were effectively blocked by the Na cations, and unlike in our work, they fixed the Na cations throughout their simulation.

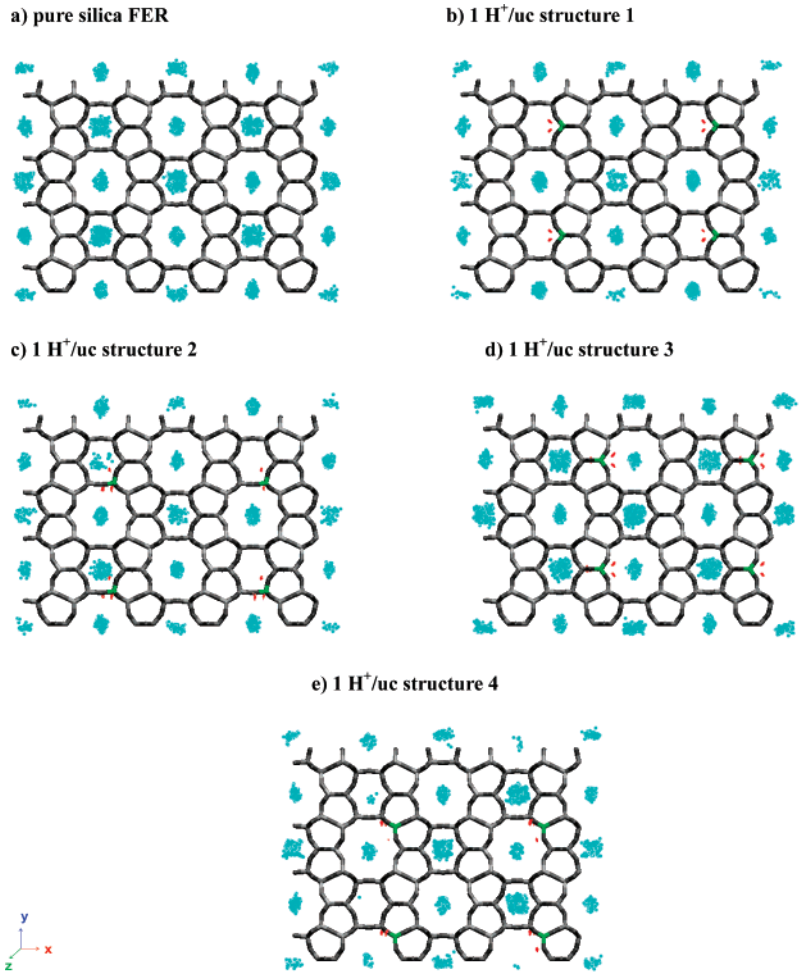

Figure 5. Distributions of butane and the non-framework protons in FER zeolites at 0.4 kPa and 333 K. The centers of mass of the butane molecules are represented by blue dots and the non-framework proton positions by red dots. The aluminum positions are indicated in green color.

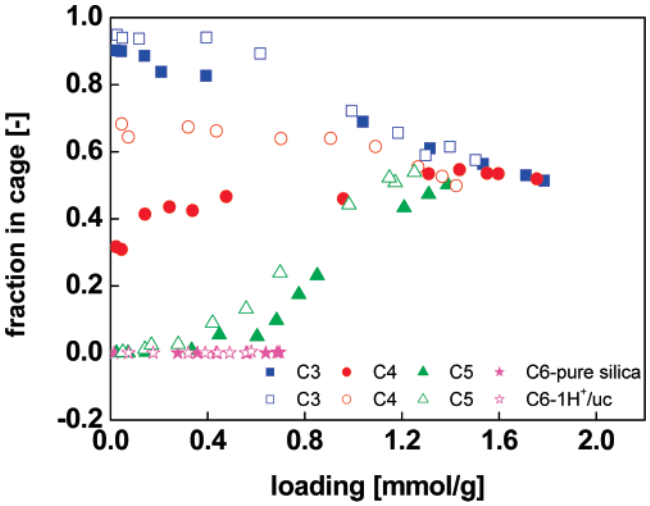

Figure 6. Fraction of the adsorbed alkane molecules located in the FER 8-ring cages as a function of loading at 333 K. The results for pure silica structure are represented by full symbols and the ones for H-FER are represented by open symbols.

Our simulation results show that by matching the simulation data with the available experimental values the most likely position of aluminum in zeolites could be identified. The aluminum position determines the cation distribution, and it is the presence and positions of the cations that can cause a difference in adsorption behavior. The Henry coefficients for FAU and LTA increase dramatically by the presence of cations, up to orders of magnitude for the longer chain lengths. As previously noted in literature, the effects of ions are 3-fold:[41,42,51] (a) ions provide additional adsorption sites, (b) ions occupy pore volume, and (c) ions can block accessible pockets and windows. FAU and LTA are examples of the first, while the second effect is here reduced because ions are allowed to occupy pore volume (the sodalite cages) that is not accessible to the bulkier alkanes. This volume effect is important in zeolites formed by channels, like MFI and MOR, and at high pressures where loadings are close to saturation. MOR is also sensitive to the third effect, showing side pockets that can be blocked.[41] In some zeolites which have very different adsorption "regions", other complications can occur. Examples include MFI, which has straight channels, zigzag channels, and intersections, and FER which has 10-ring channels and 8-ring side cages. Typically, for many adsorbates, this shows up as inflection in the adsorption isotherms[55,70−72] and/or in Henry coefficients over chain length (see Figure 1f in Supporting Information). One of the main goals of this work is to find systematic trends in this and hopefully a classification or at least same criteria to estimate the influence of ions.

For the adsorption of alkanes we found that FAU, LTA, MEL, and MFI are insensitive to the aluminum distribution, while LTL, FER, TON, and MOR belong to the sensitive class. The insensitivity of the first group originates either from large, spherical cages with a high degree of symmetry (LTA and FAU), or from structures (MEL and MFI) that have preferred aluminum positions at different locations than the alkane

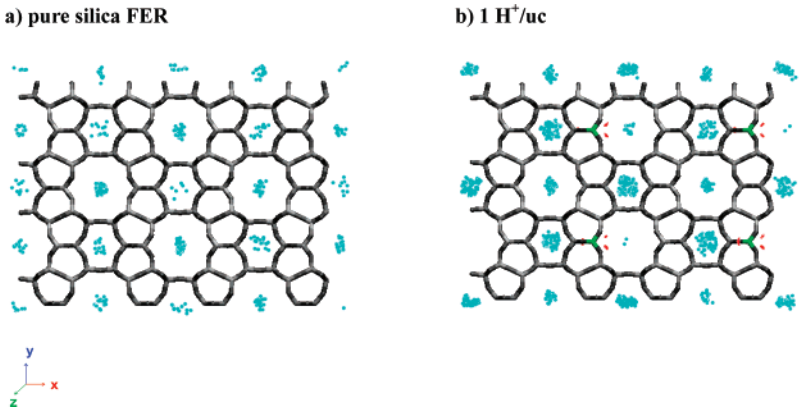

Figure 7. Distributions of butane and the non-framework protons in FER zeolites at 0.05 kPa and 333 K. The centers of mass of the butane molecules are represented by blue dots and the non-framework proton positions by red dots. The aluminum positions are indicated in green color.

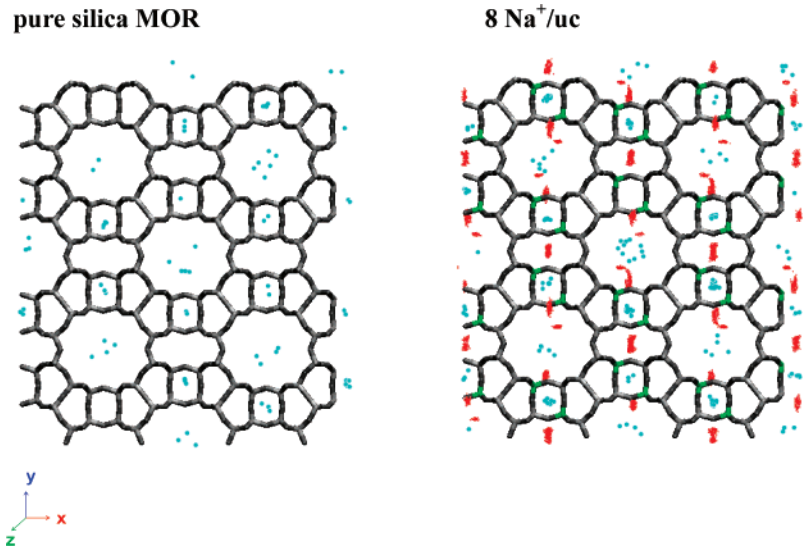

Figure 8. Distributions of methane and the non-framework sodium cations in MOR zeolites at 1 kPa and 323 K. The methane molecules are represented by blue dots and the non-framework Na^+ positions by red dots. The aluminum positions are indicated in green color.

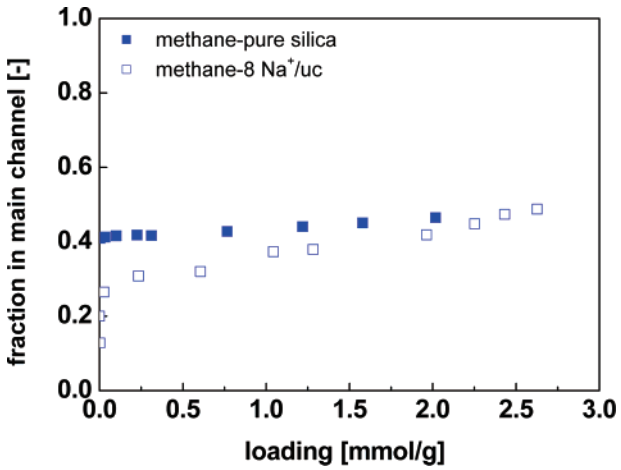

Figure 9. Fraction of the adsorbed methane located in the MOR main channels as a function of loading at 323 K. The results for pure silica structure are represented by full symbols, and the ones for Na-MOR are represented by open symbols.

adsorption sites. In MFI the preferred aluminum positions are in the big intersection, while alkanes prefer the straight channels at low loadings. LTA and FAU show a higher difference with the pure siliceous structure than MEL and MFI, mainly due to the larger amount of ions per volume present in these structures (see Figures 1a-1d in Supporting Information). The increase per carbon number is the same for MEL and MFI, but for FAU and LTA, we clearly find a change in slope. In cage-type zeolites multiple beads of the molecule have interaction with the ions. MFI and MEL have channels that tightly confine the alkanes and only the ends of the alkanes feel the ions resulting in a constant shift of the Henry coefficients as a function of carbon number. The zeolites of second group are channel systems and seem very sensitive to the positions of the aluminum, especially at low loadings. Fortunately, this is the general case. We suspect that MFI and MEL could be sensitive to other adsorbates than alkanes. This means that FAU and LTA (big cages with high degree of symmetry) are ideal to calibrate potential parameters (as we previously did[51,73]), while almost all other structures are then suitable for the "reverse engineering."[60]

We are aware that our comparisons are subject to several uncertainties as well as to the experimental and simulation errors. However, in our opinion the approach itself remains valid and very attractive as simulations and experiments advances in time. We note that the fitting procedures with the set of structures which are insensitive to the aluminum distribution are based on the same kind of experimental data and procedures. Our potentials might therefore effectively already contain a certain level of experimental error, although these of course might vary from zeolite to zeolite, and sample to sample. However, it is the best we could do using currently available experimental data,

and as soon as more experimental data becomes available we can further refine our approach.

4. Conclusions

The simulation results provided a better physical understanding of the effects of the aluminum distributions on the adsorption properties of alkanes in zeolites at a microscopic level. This work shows that the aluminum distributions in zeolites strongly affect the positions and stability of ions, which in turn influence the adsorption behavior of alkanes. Therefore, the effect of aluminum on adsorption is indirect, and it depends on the adsorbent, the ion, and the adsorbate type whether or not the adsorption is influenced. Furthermore, it should be possible, in the longer term, to use these data to more clearly delineate the relationships between the aluminum locations and the catalytic activities and selectivities of aluminosilicates.

Acknowledgment. This work is supported by the Dutch STW/CW Separation Technology program (700.56.655-DPC.6243) and the EC through Marie Curie EXT project MEXT-CT-2005-023311, by the Spanish MEC (Ministerio de Educación y Ciencia) for the projects CTQ2004-00582/BQU, CTQ2004-07730-C02-01/BQU, and VEM2003 20574 C03 01, and by the National Science Foundation (CTS-0507013). E. García-Pérez wishes to thank the MEC for a grant to prepare her Doctoral work. The authors wish to thank T. L. M. Maesen for useful discussions.

Supporting Information Available: Henry coefficients of linear alkanes in FAU, LTA, MEL, MFI, LTL, FER, and MOR zeolites at 350 K and TON zeolite at 548 K, structural information for FAU, LTA, MEL, MFI, LTL, FER, TON, and MOR zeolites, comparison of the experimental and simulated Henry coefficients of linear alkanes in H-TON zeolites at 473, 498, and 523 K, and comparison of the experimental and simulated adsorption isotherms of *n*-butane and *n*-hexane in H-FER zeolite at 333 K. This material is available free of charge via the Internet at http://pubs.acs.org.

References and Notes

(1) Krishna, R.; Smit, B.; Calero, S. *Chem. Soc. Rev.* **2002**, *31*, 185.
(2) Smit, B.; Krishna, R. *Chem. Eng. Sci.* **2003**, *58*, 557.
(3) Buttefey, S.; Boutin, A.; Mellot-Draznieks, C.; Fuchs, A. H. *J. Phys. Chem. B* **2001**, *105*, 9569.
(4) van Bokhoven, J. A.; Sambe, H.; Ramaker, D. E.; Koningsberger, D. C. *J. Phys. Chem. B* **1999**, *103*, 7557.
(5) van Bokhoven, J. A.; Koningsberger, D. C.; Kunkeler, P.; van Bekkum, H. *J. Catal.* **2002**, *211*, 540.
(6) Engelhardt, G.; Michel, D. *High Resolution Solid State NMR of Silicates and Zeolites*; John Wiley & Sons: New York, 1987.
(7) Ehresmann, J. O.; Wang, W.; Herreros, B.; Luigi, D. P.; Venkatraman, T. N.; Song, W. G.; Nicholas, J. B.; Haw, J. F. *J. Am. Chem. Soc.* **2002**, *124*, 10868.
(8) Fyfe, C. A.; Thomas, J. M.; Klinowski, J.; Gobbi, G. C. *Angew. Chem.* **1983**, *95*, 257.
(9) Joyner, R. W.; Smith, A. D.; Stockenhuber, M.; van den Berg, M. W. E. *Phys. Chem. Chem. Phys.* **2004**, *6*, 5435.
(10) Denayer, J. F.; Souverijns, W; Jacobs, P. A.; Martens, J. A.; Baron, G. V. *J. Phys. Chem. B* **1998**, *102*, 4588.
(11) Denayer, J. F.; Baron, G. V.; Vanbutsele, G.; Jacobs, P. A.; Martens, J. A. *Chem. Eng. Sci.* **1999**, *54*, 3553.
(12) Savitz, S.; Siperstein, F.; Gorte, R. J.; Myers, A. L. *J. Phys. Chem. B* **1998**, *102*, 6865.
(13) Eder, F; Lercher, J. A. *J. Phys. Chem. B* **1997**, *101*, 1273.
(14) Pieterse, J. A. Z.; Veefkind-Reyes, S.; Seshan, K.; Lercher, J. A. *J. Phys. Chem. B* **2000**, *104*, 5715.
(15) Yang, L.; Trafford, K.; Kresnawahjuesa, O.; Sepa, J.; Gorte, R. J. *J. Phys. Chem. B* **2001**, *105*, 1935.
(16) Ocakoglu, R. A.; Denayer, J. F. M.; Marin, G. B.; Martens, J. A.; Baron, G. V. *J. Phys. Chem. B* **2003**, *107*, 398.
(17) van Well, W. J. M.; Cottin, X.; de Haan, J. W.; Smit, B.; Nivarthy, G.; Lercher, J. A.; van Hooff, J. H. C.; van Santen, R. A. *J. Phys. Chem. B* **1998**, *102*, 3945.
(18) van Well, W. J. M.; Cottin, X.; de Haan, J. W.; van Santen, R. A.; Smit, B. *Angew. Chem., Int. Ed.* **1998**, *37*, 1081.
(19) Satterfield, C. N.; Frabetti, A. J., Jr. *AIChE J.* **1967**, *13*, 731.
(20) Choudhary, V. R.; Mayadevi, S.; Pai, Singh, A. *J. Chem. Soc. Faraday Trans.* **1995**, *91*, 2935.
(21) Eberly, P. E., Jr. *J. Phys. Chem.* **1963**, *67*, 2404.
(22) Xu, Q.; Eguchi, T.; Nakayama, H.; Nakamura, N. *J. Chem. Soc., Faraday Trans.* **1995**, *91*, 2949.
(23) Xu, Q.; Eguchi, T.; Nakayama, H.; Nakamura, N. *J. Chem. Soc., Faraday Trans.* **1996**, *92*, 1039.
(24) Denayer, J. F.; Baron, G. V.; Martens, J. A. and Jacobs, P. A. *J. Phys. Chem. B* **1998**, *102*, 3077.
(25) Webster, C. E.; Cottone, A. III; Drago, R. S. *J. Am. Chem. Soc.* **1999**, *121*, 12127.
(26) Macedonia, M. D.; Moore, D. D.; Maginn, E. J. *Langmuir* **2000**, *16*, 3823.
(27) Yamazaki, T.; Hasegawa, K.; Honma Ken-ichi and Ozawa S. *Phys. Chem. Chem. Phys.* **2001**, *3*, 2686.
(28) Yuvaray, S.; Chang, T. H.; Yeh, C. T. *J. Phys. Chem. B* **2003**, *107*, 4971.
(29) Salla, I.; Montanari, T.; Salagre, P.; Cesteros, Y. and Busca G. *J. Phys. Chem. B* **2005**, *109*, 915.
(30) Delgado, J. A.; Uguina, M. A.; Gomez, J. M. *Stud. Surf. Sci. Catal., A* and *B* **2005**, *158*, 1065.
(31) Maesen, T. L. M.; Schenk, M.; Vlugt, T. J. H.; de Jonge, J. P.; Smit, B. *J. Catal.* **1999**, *188*, 403.
(32) Schenk, M.; Smit, B.; Vlugt, T. J. H.; Maesen, T. L. M. *Angew. Chem., Int. Ed.* **2001**, *40*, 736.
(33) Domokos, L.; Lefferts, L.; Seshan, K.; Lercher, J. A. *J. Catal.* **2001**, *203*, 351.
(34) Raybaud, P.; Patrigeon, A.; Toulhoat, H. *J. Catal.* **2001**, *197*, 98.
(35) Lu, L.-H.; Wang, Q.; Liu, Y.-C. *Acta Chim. Sinica* **2003**, *61*, 1232.
(36) Ndjaka, J.-M. B.; Zwanenburg, G.; Smit, B.; Schenk, M. *Microporous Mesoporous Mater.* **2004**, *68*, 37.
(37) van Well, W. J. M.; Cottin, X.; Smit, B.; van Hooff, J. H. C.; van Santen, R. A. *J. Phys. Chem. B* **1998**, *102*, 3952.
(38) Pascual, P.; Boutin, A. *Phys. Chem. Chem. Phys.* **2004**, *6*, 2015.
(39) Pascual, P.; Boutin, A.; Ungerer, P.; Tavitian, B.; Fuchs, A. H. *Mol. Simul.* **2004**, *30*, 593.
(40) Smit, B.; den Ouden, C. J. J. *J. Phys. Chem.* **1988**, *92*, 7169.
(41) Beerdsen, E.; Smit, B.; Calero, S. *J. Phys. Chem. B* **2002**, *106*, 10659.
(42) Liu, B.; Smit, B. *Phys. Chem. Chem. Phys.* **2006**, *8*, 1852.
(43) Koranyi,T. I.; Nagy, J. B. *J. Phys. Chem. B* **2005**, *109*, 15791.
(44) Bodart, P.; Nagy, J. B.; Debras, G.; Gabelica, Z.; Jacobs, P. A. *J. Phys. Chem.* **1986**, *90*, 5183.
(45) Takaishi, T.; Kato, M.; Itabashi, K. *Zeolites* **1995**, *15*, 21.
(46) Peterson, B. K. *J. Phys. Chem. B* **1999**, *103*, 3145.
(47) Herrero, C. P.; Utrera, L.; Ramirez, R. *Phys. Rev. B* **1992**, *46*, 787.
(48) Vega, A. J. *J. Phys. Chem.* **1996**, *100*, 833.
(49) Ding, D. T.; Li, B. H.; Sun, P. C.; Jin, Q. H.; Wang, J. Z. *Zeolites* **1995**, *15*, 569.
(50) International Zeolite Association, Structure Commission, http://www.iza-structure.org.
(51) Calero, S.; Dubbeldam, D.; Krishna, R.; Smit, B.; Vlugt, T. J. H.; Denayer, J. F. M.; Martens, J. A.; Maesen, T. L. M. *J. Am. Chem. Soc.* **2004**, *126*, 11377.
(52) Maesen, T. L. M.; Schenk, M.; Vlugt, T. J. H.; Smit, B. *J. Catal.* **2001**, *203*, 281.
(53) Dubbeldam, D.; Beerdsen, E.; Vlugt, T. J. H.; Smit, B. *J. Chem. Phys.* **2005**, *122*, 224712.
(54) Vlugt, T. J. H.; Schenk, M. *J. Phys. Chem. B* **2002**, *106*, 12757.
(55) Dubbeldam, D.; Calero, S.; Vlugt, T. J. H.; Krishna, R.; Maesen, T. L. M.; Beerdsen, E.; Smit, B. *Phys. Rev. Lett.* **2004**, *93*, 088302.
(56) Dubbeldam, D.; Calero, S.; Vlugt, T. J. H.; Krishna, R.; Maesen, T. L. M.; Smit, B. *J. Phys. Chem. B* **2004**, *108*, 12301.
(57) Calero, S.; Lobato, M. D.; García-Pérez, E.; Mejías, J. A.; Lago, S.; Vlugt, T. J. H.; Maesen, T. L. M.; Smit, B.; Dubbeldam, D. *J. Phys. Chem. B* **2006**, *110*, 5838.
(58) Ryckaert, J. P.; Bellemans, A. *Faraday Discuss. Chem. Soc.* **1978**, *66*, 95.
(59) Frenkel, D.; Smit, B. *Understanding Molecular Simulations: From Algorithms to Applications*, 2nd ed.; Academic Press: San Diego, 2002.
(60) García-Pérez, E.; Dubbeldam, D.; Liu, B.; Smit, B.; Calero, S. *Angew. Chem., Int. Ed.* **2007**, *46*, 276.
(61) Maesen, T. L. M.; Beerdsen, E.; Calero, S.; Dubbeldam, D.; Smit, B. *J. Catal.* **2006**, *237*, 278.
(62) Schelenker, J. L.; Pluth, J. J.; Smith, J. V. *Mater. Res. Bull.* **1968**, *13*, 169.
(63) Meier, W. M.; Gramlich, V. *Z. Kristallogr.* **1978**, *147*, 329.

(64) Derouane, E. G. ; Fripiat, J. J. *Proceedings of the 6th International Zeolite Conference*, Reno, NV, July 10−15, 1983; Olson, D. H., Bisio, A., Eds.; Butterworths: Guilford, 1984; p 717.

(65) Debras, G.; Nagy, J. B.; Gabelica, Z.; Bodart, P.; Jacobs, P. A. *Chem. Lett.* **1983**, 199.

(66) Maurin, G.; Senet, P.; Devautour, S.; Gaveau, P.; Henn, F.; van Doren, V. E.; Giuntini, J. C. *J. Phys. Chem. B* **2001**, *105*, 9157.

(67) Maurin, G.; Bell, R. G.; Devautour, S.; Henn, F.; Giuntini, J. C. *J. Phys. Chem. B* **2004**, *108*, 3739.

(68) Meier, W. M. *Z. Kristallogr.* **1961**, *115*, 439.

(69) Nivarthi, S. S.; Van Tassel, P. R.; Davis, H. T.; McCormick, A. V. *J. Chem. Phys.* **1995**, *103*, 3029.

(70) Smit, B.; Maesen, T. L. M. *Nature* **1995**, *374*, 42.

(71) Vlugt, T. J. H.; Zhu, W.; Kapteijn, F.; Moulijn, J. A.; Smit, B.; Krishna, R. *J. Am. Chem. Soc.* **1998**, *120*, 5599.

(72) Vlugt, T. J. H.; Krishna, R.; Smit, B. *J. Phys. Chem. B* **1999**, *103*, 1102.

(73) García-Pérez, E.; Dubbeldam, D.; Maesen, T. L. M.; Calero, S. *J. Phys. Chem. B* **2006**, *110*, 23968.